Seismic performance of non-ductile detailing RC frames: An experimental investigation

Banu A. Hidayat[1,2], Hsuan-Teh Hu[1,3], Fu-Pei Hsiao[*1,4], Ay Lie Han[2], Panapa Pita[1] and Yanuar Haryanto[1,5]

[1]*Department of Civil Engineering, College of Engineering, National Cheng Kung University,*
No. 1 University Road, Tainan, 701, Taiwan (R.O.C.)
[2]*Department of Civil Engineering, Faculty of Engineering, Diponegoro University,*
Jalan Prof. Soedarto, Tembalang, Semarang, 50375, Indonesia
[3]*Department of Civil and Disaster Prevention Engineering, College of Engineering and Science, National United University,*
No. 2, Lien Da, Nan Shih Li, Miaoli, 36063, Taiwan (R.O.C.)
[4]*National Center for Research on Earthquake Engineering,*
200 Sec. 3, Xinhai Road, Taipei, 10668, Taiwan (R.O.C.)
[5]*Department of Civil Engineering, Faculty of Engineering, Jenderal Soedirman University,*
Jalan Mayjen. Sungkono KM 5, Blater, Purbalingga, 53371, Indonesia

Abstract. Non-ductile detailing of Reinforced Concrete (RC) frames may lead to structural failure when the structure is subjected to earthquake response. These designs are generally encountered in older RC frames constructed prior to the introduction of the ductility aspect. The failure observed in the beam–column joints (BCJs) and accompanied by excessive column damage. This work examines the seismic performance and failure mode of non-ductile designed RC columns and exterior BCJs. The design was based on the actual building in Tainan City, Taiwan, that collapsed due to the 2016 Meinong earthquake. Hence, an experimental investigation using cyclic testing was performed on two columns and two BCJ specimens scaled down to 50%. The experiment resulted in a poor response in both specimens. Excessive cracks and their propagation due to the incursion of the lateral loads could be observed close to the top and bottom of the specimens. Joint shear failure appeared in the joints. The ductility of the member was below the desired value of 4. This is the minimum number required to survive an earthquake with a similar magnitude to that of El Centro. The evidence provides an understanding of the seismic failure of poorly detailed RC frame structures.

Keywords: columns; beam-column joints; quasi-static cyclic test; non-ductile detailing; plastic hinges

1. Introduction

As Taiwan is situated on the Circum-Pacific seismic belt, seismic activity is one of Taiwan's main natural hazards. Taiwan has suffered extensive damage from earthquakes in the past, which have caused thousands of injuries and deaths of people. In addition, thousands of buildings were collapsed by the Chi-Chi earthquake in 1999, the 2016 Meinong earthquake, and other strong earthquakes. Of this number, most of the collapsed buildings were constructed of reinforced concrete (RC) frames (Tsai *et al.* 2000, Xue 2000, Zepeda and Hagen 2016, Shen *et al.* 2019, Shen *et al.* 2018).

The damage was commonly existed in the beam–column joints (BCJs) followed by excessive column damage or non-ductile detailing on existing concrete frame structures. This defect commonly occurred in the first story of buildings with a larger opening and higher story height. This condition leads to lower structural stiffness and strength and causes the soft-story mechanism. Furthermore, non-ductile
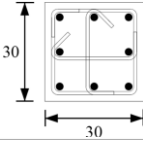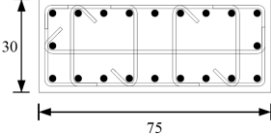
detailing concrete appeared in BCJ failures without transverse reinforcement, in shear failures in shear critical columns, and in axial demand failures in corner columns (Tsai *et al.* 2000, Sharma *et al.* 2013, Zepeda and Hagen 2016, Shen *et al.* 2018, Shen *et al.* 2019).

The seismic experiences resulted in increasing awareness of the vulnerabilities of RC buildings in Taiwan. The assessment of the seismic adequacy of existing buildings is taken into account (Hsu and Pham 2019, Yön 2020), causing the stricter building design code (Tudjono *et al.* 2015, Tudjono *et al.* 2018, Surana 2019) and the strengthening system of the building (Kalogeropoulos *et al.* 2019, Yang and Zhang 2019). Thus, collapse prevention of RC components of multi-story buildings has become a favorite issue in the earthquake engineering research area, which is continuously growing due to the numerous occurrence of earthquakes (Hsiao *et al.* 2008, Lu *et al.* 2013, Hsiao *et al.* 2015, Cardone and Flora 2016, Barbagallo *et al.* 2017, Shiravand *et al.* 2017, Esteghamati *et al.* 2018, Haryanto *et al.* 2019, Xiao *et al.* 2019).

Numerous researches have investigated the seismic performance of RC columns characterized by deficiency related to poor detailing, which leads to non-ductile behavior. Different amounts and detailing layouts of transverse reinforcements used in column specimens have

---

*Corresponding author, Researcher Fellow
E-mail: fphsiao@ncree.narl.org.tw

Table 1 Details of RC column and BCJ specimens (units: mm)

	Longitudinal bars	Stirrups bars	Crossties bars	Cross-sectional area
Column specimens				
C-A 300x300	8 D19	D10-120	D10-240	
C-B 300x750	20 D19	D10-120	D10-240	
BCJ specimens				
C-A	8 D19	D10-125	D10-240	(the same as the C-A and C-B
C-B	20 D19	D10-125	D10-240	in column specimens)
Beam 250x400	6 D19 top 4 D19 bottom	D10-150	-	
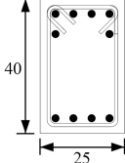
been investigated (Sheikh *et al.* 1994, Mo and Wang 2000, Benavent-Climent and Zahran 2010, Liao *et al.* 2017, Rajput and Sharma 2017). Larger spacing of tie bars allows dilation of the concrete core and exhibits poor performance against cyclic loading. In addition, a transverse reinforcement detailing layout is a crucial factor to ensure ductile behavior in RC columns. The added confinement provided by transverse bars enhances the crack prevention, energy dissipation capacity, and strength of column specimens.

Since the cyclic behaviors of RC BCJs are also important, a number of experimental studies of poorly detailed exterior joints have been conducted. Park and Paulay (1973) performed one of the earlier tests on external RC BCJs under seismic load, which focused on an impact assessment of transverse rebar in terms of loading and ductility. Following this, other researchers carried out investigations of joint cores involving various parameters, including the beam reinforcement ratio, joint geometries, joint shear demands, and anchorage details (Kaku and Asakusa 1991, Pantazopoulou and Bonacci 1992, Hakuto *et al.* 2000, Pantelides *et al.* 2002, Pampanin *et al.* 2003, Yen and Chien 2004, Wong 2005, Haach *et al.* 2008, Lu *et al.* 2012, Shafaei *et al.* 2014, Li *et al.* 2015, Faleschini *et al.* 2017). The results showed that joints with substandard details were primarily failed by bond-slip and joint shear mode. The decreased energy dissipation capacity for non-seismically detailed specimens was also reported. An appropriate anchorage length of the end hook bars and the presence of transversal reinforcement within the joint core are crucial for providing bonding to enhance the performance of a BCJ component. The implications of bond degradation consist of pinching the hysteresis curves of force versus story drift, modifying the shear transfer mechanism in the joint core, expanding the slip deformation at the interface of beam and column, and reducing the flexural strength of the adjacent RC members (Kaku and Asakusa 1991).

Despite a large number of investigations on the seismic performance of non-ductile detailing RC frames being undertaken, sufficient understanding of the behavior of such frames is critical. Further, it is important to investigate how the various parameters influence the performance of non-ductile RC frames, which focused on the shaking table test of a half-scale three-story building referred to the Weiguan Jinlong tower in Tainan City, Taiwan. The structural design of this building did not consider the ductility requirements and the building was not properly designed to be resistant to earthquake. Consequently, it collapsed during the 2016 Meinong earthquake. Particularly, this paper will broaden the results of the previous research conducted by Shen *et al.* (2018).

The parametric study of the current work is extended to the more detailed performance and behavior of the RC members subjected to seismic load. Afterwards, the non-ductile and poorly designed RC columns and BCJs were investigated using the quasi-static testing method, performed by the Multi-Axial Testing System (MATS) in the National Center for Research on Earthquake Engineering (NCREE) Laboratory in Tainan City. The prototypes are taken from the first-floor external columns and the exterior BCJ components of the three-story building, since they are having greater vulnerability compared to other RC members. The specimens were casted with exactly the same dimensions, the reinforcement configurations, and the material properties of the columns and BCJs in the three-story building tested in the shaking table test.

2. Experimental program

2.1 Specimen configurations

The column specimens were constructed with a 2,600 mm length and different cross-sectional areas of 300 × 300

(a) The BCJ-A specimen

(b) The BCJ-B specimen

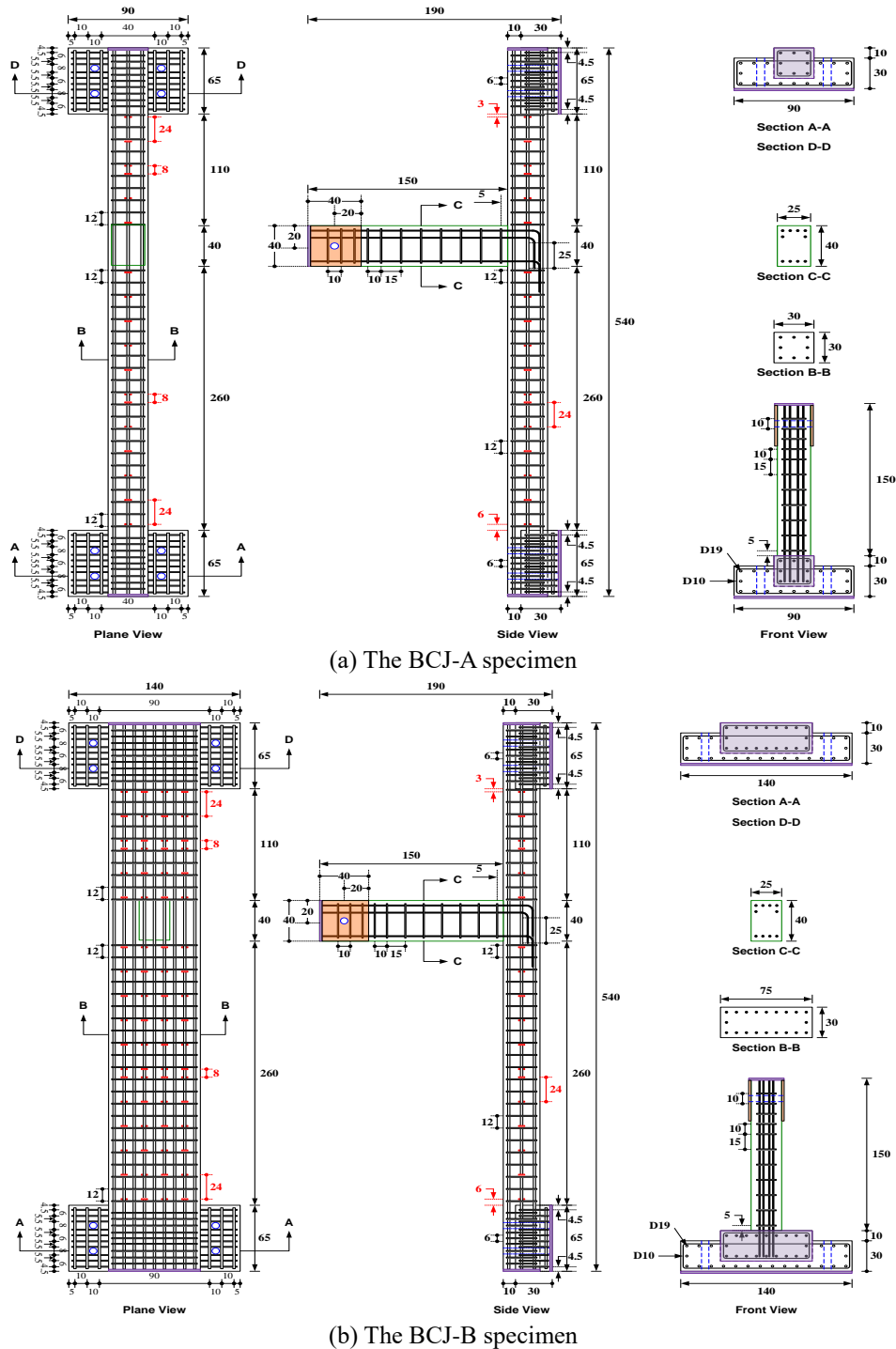Fig. 1 The reinforcement configuration of the BCJ specimens for the quasi-static test (units: cm)

mm for the small column denoted as C-A and 300 × 750 mm for C-B symbolized the large column. For the BCJ specimens, two columns with lengths of 4,100 mm were connected to the beam, which had an area of 250 × 400 mm and 1,500 mm length, and were denoted as BCJ-A and BCJ-B, respectively. Table 1 and also Fig. 1 show the details and configurations of longitudinal and transversal reinforcement of the RC specimens for the quasi-static test. The compressive strength of the concrete, following ASTM-C39 (2020) testing, was 21.96 MPa at 28-day. Fig. 2 illustrates

that the reinforcements were tested and the obtained elastic modulus, yield strength, and ultimate strength were found to be 355.45 GPa, 450 MPa, and 634 MPa for the 19-mm-diameter bar and 208.77 GPa, 355 MPa, and 471 MPa for the 10-mm-diameter bar, respectively. This value can be considered as a low grade for the steel reinforcement. The schematic configuration of the MATS was displayed in Fig. 3.

The pre-ductile reinforcement details on columns were represented by a wide transverse reinforcement, with 120
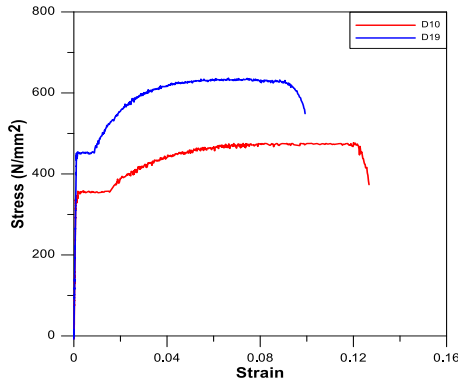
Fig. 2 Tensile test result of steel reinforcement
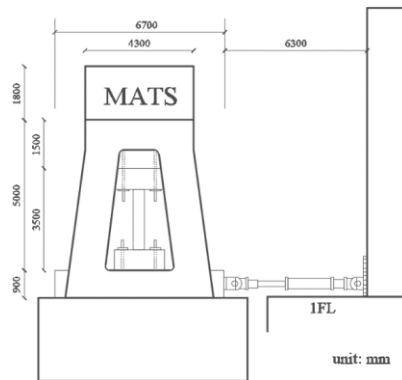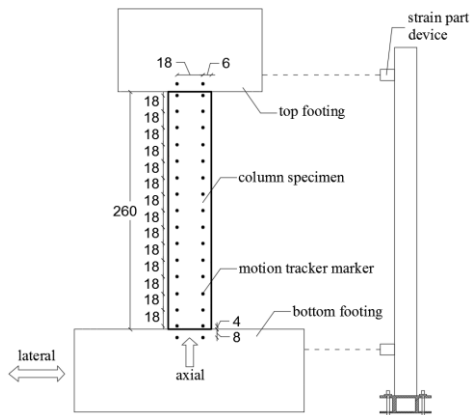

Fig. 3 Schematic figure of MATS in NCREE Laboratory

(a) Schematic test set up for the column (units: cm)   (b) C-A specimen   (c) C-B specimen
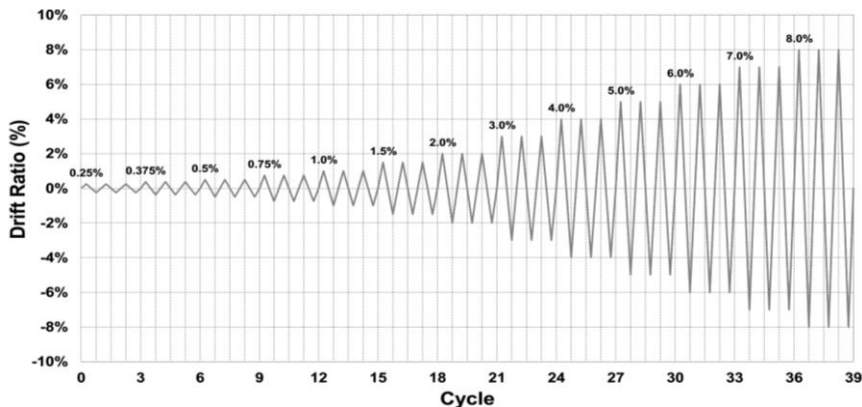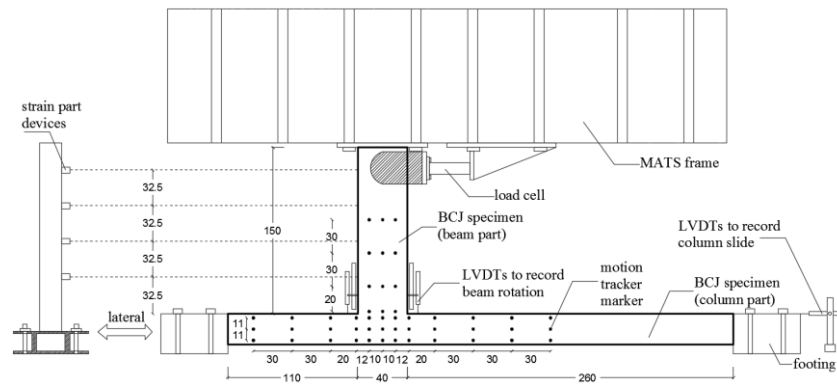
Fig. 4 Column test setup using MATS

Fig. 5 Loading protocol applied to both column specimens

(a) Schematic test set up for the BCJ specimens (units: cm)

(b) Side view of the BCJ specimen

Fig. 6 Test setup for the BCJ specimens using MATS

(a) For BCJ-A specimen
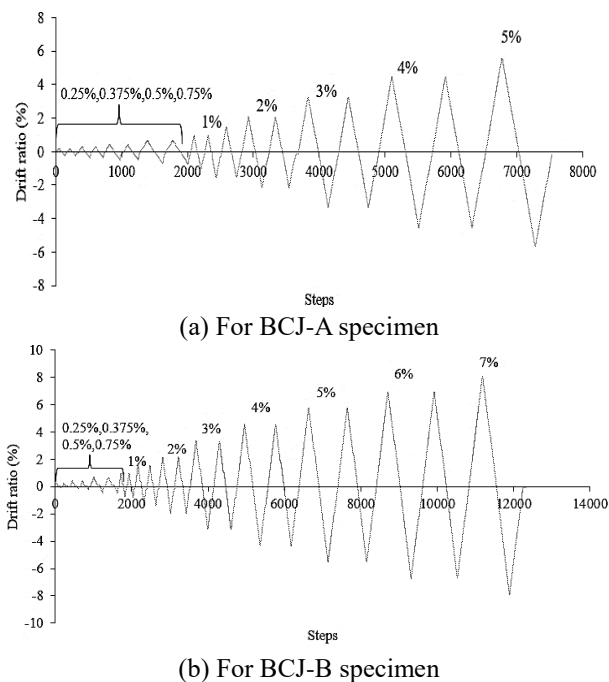

(b) For BCJ-B specimen

Fig. 7 Loading protocol applied to both BCJ specimens

and 250 mm spacing for the stirrup and cross-ties, respectively. The 20-mm concrete cover was also smaller than the cover specified in ACI 318-19 (2019). However, both columns and beams were designed with non-rigid reinforcement details with ratios of 2.53 and 2.85%, respectively, as mentioned in Table 1, which complied with

the minimum requirement of the ACI 318-19 (2019). The poor design of the BCJ mechanisms was represented by a lack of shear reinforcement and poor anchorage inside the joint core, and the behavior of a strong beam with a weak column was applied.

2.2 Test setup and test procedure

2.2.1 Columns

The columns were tested in a vertical position inside the MATS to investigate the cyclic behavior, as displayed in Fig. 4, respectively for C-A and C-B. During the test, the deformations of the column are monitored by a variety of advanced optical measurement sensor systems, including 30 motion tracker devices to measure the deformation of the column near the bases and two strain part devices which were installed at both column ends to measure the column displacement.

In each specimen, a constant axial load of 237 kN was induced, which was equal to approximately 12 and 6% of f'_c A_g for C-A and C-B specimens, respectively, where f'_c denotes the compressive strength of the concrete and A_g of the cross-section area of the column. The axial load is considered from the specimen weight and the additional mass from the three-story building specimen in the shaking table test, which taken only for the first-floor column. After the load application was achieved, MATS was used to perform the quasi-static test on the bottom of the column through the displacement-controlled mode hydraulic actuator. The loading protocol has been derived from ACI

(a) C-A specimen at an 8% drift ratio   (b) C-B specimen at a 4% drift ratio

Fig. 8 Final crack patterns of the column specimens

(a) BCJ-A specimen at a 5% drift ratio   (b) BCJ-B specimen at a 7% drift ratio

Fig. 9 Final crack pattern of the beam–column joint

374.1-05 code (2019). As stated in Fig. 5, three fully reversed cycles were added at each loading stage.

2.2.2 Beam–column joints

Both BCJ specimens, as shown in Fig. 6, were examined in the MATS with the column sitting horizontally and the beam was in the vertical position. In order to simulate support conditions on the beam and both ends of the columns, the hinge was constructed as a swivel connector on the beam positioned 1,300 mm from the column surface and was linked to a load cell. The footing was designed to allow the column to display vertical deformation, and both joints were also designed with hinge mechanisms to account for the rotation effect. The lateral load of the machine is placed in the bottom part of the specimen.

The specimens were fitted with strain gauge devices mounted in the critical position of reinforcements to measure the strain, strain part devices installed to evaluate the beam deflection, the Linear Variable Displacement Transducer (LVDT) to observe the column slide and beam rotation, and motion tracker devices to record the joint distortion. The quasi-static test was applied to the MATS to examine the cyclic behavior of the joint rather than the beam itself. The lateral loading protocol was in accordance

with ACI 374.2R-13 (2013), consisting of displacement-controlled steps starting at 0.25, 0.375, 0.5, 0.75, 1, 1.5, 2, 3, 4, 5, 6, and 7%. However, the loading protocol on the BCJ-A specimen ended at a drift ratio of 5%, when failure occurred. The loading test for both specimens can be viewed in Fig. 7.

3. Experimental results

3.1 Crack propagation and failure mechanism

The crack propagation for the C-A and C-B specimens started from the appearance of minor flexural cracks at the bottom end of specimens, which occurred slowly at 0.5 and 0.25% drift ratios, respectively, and then continued with diagonal cracks at drift ratios of 1 and 0.5%, respectively. The width of the existing cracks became larger, as the drift ratio increased. The two specimens reached their maximum lateral loads of 96.86 kN for C-A and 225.24 kN for C-B, respectively, at a 3% drift ratio. However, the experiment was continued at drift ratios of 8 and 4% for each column specimen. The test ended more quickly for C-B due to rapid propagation and increases in crack width, indicating an inability to control cracks.

When the test of the C-A specimen ended, the widest crack existed at the intersection between the column and the bottom base, indicating that the longitudinal bars slip occurred. In addition, for the C-B specimens, the widest crack occurred near to the top in the form of splitting cracks. The C-A specimen failed in the axial flexural mode, whereas the C-B specimen was governed by shear failure. The final crack patterns of the two column specimens are exhibited in Fig. 8. The C-A specimen responded in a ductile manner compared to the C-B specimen.

However, in both BCJ specimens, the first cracks formed in the joint area of the BCJ-A specimen and on the column face 700 mm from the joint zone of the BCJ-B specimen at a drift ratio of 0.25%. This was in the form of 0.25 mm wide flexural cracks. There was opening of the diagonal cracks due to concrete crushing, bonding deterioration of the beam bottom reinforcement, and the lateral ultimate load degradation. The splitting cracks around the joint region through the column caused the anchorage length of the beam near the column face to become inadequate. The wider diagonal cracks at the bottom of the joint area indicates the degradation of the joint stiffness and moment resisting capacity. As the drift ratio gradually increased, the inelastic rotation from the beam to the joint made the condition of the joints become more and more disrupted due to the existing cracks.

The BCJ-A reached the maximum load of 100.40 kN, corresponding to a drift ratio of 2% along the positive direction, which continued until the test terminated at a 5% drift ratio. Moreover, the maximum lateral load of the BCJ-B was 157.57 kN, associated to a drift ratio of 3% in the positive direction, and the test finished at a drift ratio of 7%. The primary failure mode of both specimens was driven by diagonal shear cracking in the joint zone, due to an insufficient number of joint shear reinforcements. The final
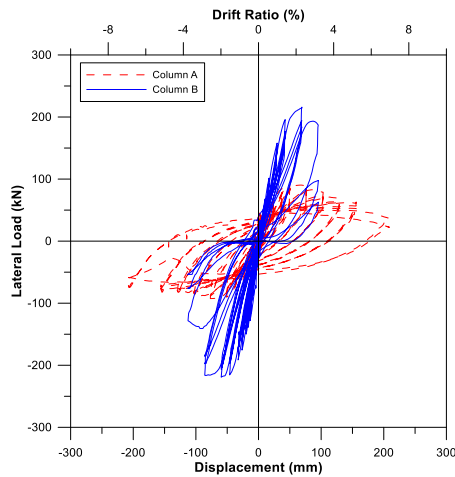
Fig. 10 Lateral load versus displacement with corresponding drift ratio hysteretic response of the C-A and C-B specimens

Fig. 11 Lateral load versus displacement with corresponding drift ratio hysteretic response of the BCJ-A and BCJ-B specimens

crack development of the BCJ-A and BCJ-B specimens is shown in Fig. 9.

3.2 Hysteretic response

The hysteretic curve pattern for the C-A and C-B specimens, as shown in Fig. 10, has a different behavior response. Column C-B has lower lateral drift and higher strength than the C-A specimen. In addition, the C-A specimen exhibited a more ductile hysteretic loop with flexural failure, indicated by a gradual 12% drop in strength when the maximum load was reached. In contrast, the C-B specimen showed a 48% drop in strength when it passed beyond the maximum load. This 48% strength drop condition was quite tremendous due to a considerable degradation amount of stiffness and strength as the displacement increased, which was mainly associated to shear failure.

As for the BCJ-A and BCJ-B specimens, the hysteretic curves behaved similarly in response, as shown in Fig. 11. However, both specimens exhibited a minor stiffness and strength deterioration, indicated by the load drop when the maximum load was reached. This degradation occurred continuously as the input displacement increased until the specimen failed in flexural shear in the joint region.

Based on ACI 374.2R-13 (2013), RC frames are expected to display a permanent drift ratio of up to 4%. This value is the limit range of structural performance under a discrete level of collapse prevention that RC structures experience under seismic loading and can be considered as an ultimate failure. From Figs. 10 and 11, it was observed that less exact adherence to the provisions was obtained for the C-B specimen, as it failed prior to the 4% drift ratio, whereas the C-A specimen and both BCJ specimens followed the provisions.

3.3 Ductility

Ductility can be defined as the ability of materials or structures to resist inelastic deformation prior to collapse
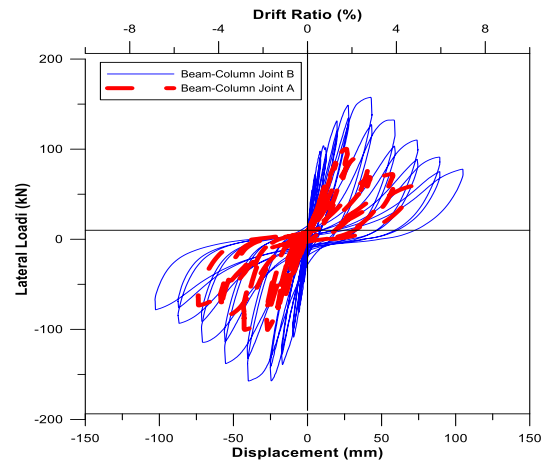
without experiencing a considerable drop of strength capacity. It also provides the ability to resist sudden local impact loading and to dissipate energy during cyclic loading. By having good ductility, the structure can allow redistribution of stress and increasing deflections to warn against failure (Morais and Burgoyne 2001).

The ductility factor is described as the ratio of ultimate displacement to yield displacement of the section. The displacement at yielding needs to be measured to assess the ductility factors; however, this also creates difficulties since the load–displacement curve of RC members does not have a well-defined yield point due to the non-linear behavior of the materials. As a result, Paulay and Priestley (1992) proposed a procedure for evaluating the parameters of ductility through the idealization of bilinear load–displacement response.

The ductility factor can be determined by using Eq. (1)

$$\mu = \delta_u / \delta_y \qquad (1)$$

The ultimate displacement, denoted as δ_u, is a value that corresponds to either a 20% decrease in maximum load, longitudinal reinforcement buckling, or the reinforcement fracturing, whichever happens first. However, yield displacement, denoted as δ_y, is referred by establishing a straight line from the origin point to the point where the first yield of the longitudinal reinforcement of the beam occurred on a load–displacement envelope curve or a 75% reduction of the ultimate load (Paulay 1989, Paulay and Priestley 1992, Huang *et al.* 2018).

The ductility factor can be determined from the envelope curve of load–displacement response by using this method. Fig. 12 shows the curve of the load–displacement relation along the positive direction in the column and BCJ specimens, respectively. In addition, the calculation of the ductility factor is shown in Table 2.

As mentioned in Table 2, there is a quite substantial difference in ductility factor and ultimate load between both specimens. The C-A specimen exhibits a higher ductility capacity of 2.50 compared to the C-B specimen, which has a ductility capacity of 1.87. The difference was estimated to
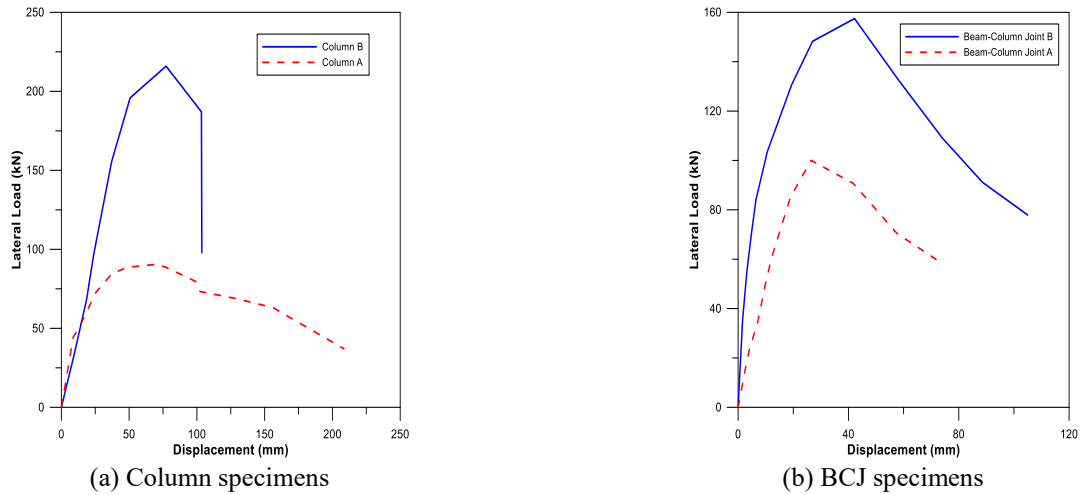
(a) Column specimens

(b) BCJ specimens

Fig. 12 The load–displacement responses comparison for the column and BCJ specimens

Table 2 The ductility factors for the column and BCJ specimens

Specimens	P_u (kN)	δ_y (mm)	δ_u (mm)	$\mu = \delta_u / \delta_y$
C-A	90	40	100	2.50
C-B	216	55	103	1.87
BCJ-A	100	24	50	2.08
BCJ-B	155	19	61	3.21

be a 25% higher ductility factor for the C-A specimen. In the case of the BCJ specimens, it can be observed that the BCJ-B specimen displays a 35% higher ductility factor than the BCJ-A specimen due to the larger cross-section area of the column. However, all the specimens' ductility capacities were lower than the limit of 4 to 6 suggested by Blume *et al.* (1961) in order to survive an earthquake that has a magnitude similar to El-Centro earthquake.

3.4 Dissipated energy and elastic stored energy

Dissipated energy is one of the most important measures for evaluating the fracture work of components during seismic loading (Qeshta *et al.* 2014) and measured based on the area under the load–displacement curve. Fig. 13 displays that the amount of dissipated energy obtained for all specimens is associated with a displacement of around 70 mm attained during the test. The value was taken from the displacement point when the maximum lateral load was achieved in the hysteresis loop, as mentioned in Figs. 10 and 11. As shown in Fig. 13(a), the C-B specimen showed 47% more dissipated energy than the C-A specimen, due to the different geometric sectional areas of the specimens, even though they had the same material properties and reinforcement details.

However, among the BCJ specimens, the BCJ-B specimen showed 30% higher dissipated energy compared to the BCJ-A specimen, as shown in Fig. 13(b). This further proved the concept suggesting that a strong column with a weak beam mechanism, as in the BCJ-B specimen, is more effective due to the ability to resist more lateral movement under seismic loading. The increase in dissipated energy is marked by the delay in crack propagation and the yield and
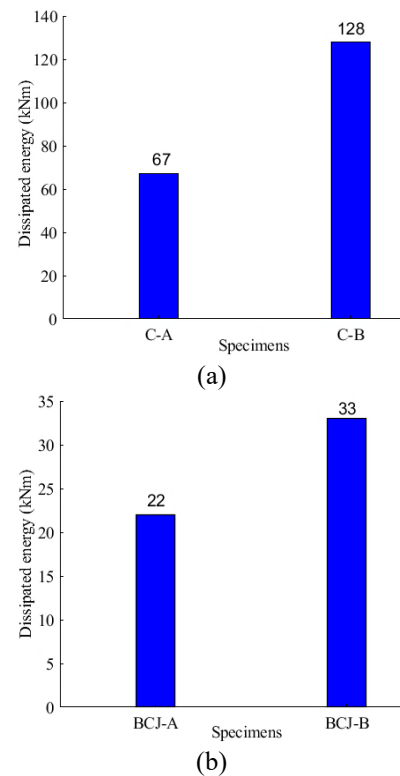

(a)

(b)

Fig. 13 Dissipated energy response for (a) column and (b) beam–column joint specimens

ultimate load enhancement.

3.5 Beam rotation

In this study, two LVDTs were mounted on either side of the beam located on top of the column near the joint region, to measure rotation of the beam in the plastic hinge region. Fig. 14 presents the curve of positive beam rotation versus the applied moment for the BCJ-A and BCJ-B specimens, respectively. The applied moment can be obtained by multiplying the induced lateral load by a beam length taken to the hinge position. In addition, beam rotation, denoted as rad, is determined using Eq. (2), where
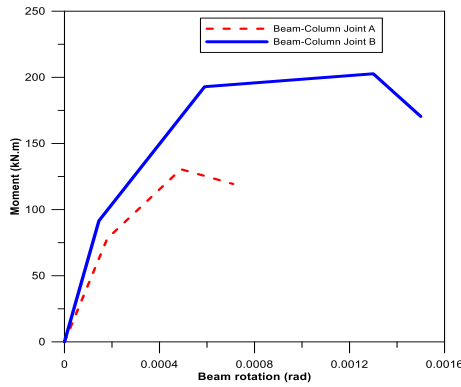
Fig. 14 The curve of beam moment versus beam rotation for the BCJ specimens

ΔL_1 and ΔL_2 stand for shortening and elongation recorded by the LVDTs and L0 is the length of the beam to hinge position.

$$rad = \frac{average(\Delta L_1 + \Delta L_2)}{L_0} \qquad (2)$$

The results obtained from Fig. 14 indicated a high amount of beam rotation for the BCJ-A specimen, due to the weak column with a strong beam mechanism. This induces lower stiffness in BCJ-A compared with BCJ-B. In addition, both specimens yield about the same rotation at 0.0002 rad with different applied moments of 70 and 90 kNm for BCJ-A and BCJ-B, respectively.

3.6 Reinforcement strains analysis

Forty-six electrical resistance strain gauges were installed to the BCJ specimens, distributed at the top and bottom of the longitudinal and transversal bars of the beam, shear reinforcement at the inside of the joint core, and the column's longitudinal and transverse bars. The strain gauges were fitted to calculate the local strain on reinforcement during cyclic loading and were compared with yield strains of approximately 1,270 and 1,710 micro-strains, for the longitudinal and transversal bars, respectively. The placement of the strain gauges used in this section is depicted in Fig. 15.

Fig. 16 displays the measured normalized strains in the beam's longitudinal rebar in the plastic hinge region, located 25 mm from the column face. Both top beam reinforcements yielded during the negative cyclic loading and gradually decreased to a positive cyclic loading at a specific drift ratio, due to the loss of tensile strength, as presented in Figs. 16(a) and 16(b). In addition, the bottom beam reinforcement had yielded during the negative cyclic loading, and the magnitude of the compressive strain gradually increased and became tensile due to the local interface of a pull-out crack, as shown in Fig. 16(c).

The normalized strain of the beam stirrup located 200 mm from the column face is shown in Fig. 17. The result displays that the stirrup at the plastic hinge of the BCJ-B specimen yielded during positive cyclic loading, whereas BCJ-A did not yield due to immediate joint failure of the
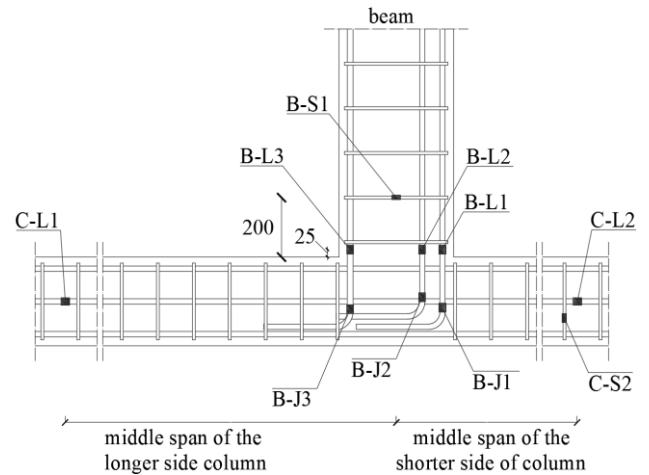

Fig. 15 The location of strain gauge used in the analysis (units: mm)

beam stirrups. The BCJ-B specimen showed a gradual increased in compressive strain, which became tensile and reached a yielding point at a positive drift ratio of 2%. It was indicated by the residual plastic strain that developed, which gradually decreased after passing a positive drift ratio of approximately 3%. The strain reduction corresponds to a peak reduction in the cyclic load.

Fig. 18 displays the normalized strains at the middle longitudinal rebar on the short and longer side spans of the column, located between and close to the joint zone. The BCJ-B specimen exhibited tensile strain and exceeded the yield point at specific negative and positive drift ratios, whereas BCJ-A was failed below the yield point due to the early development of joint failures, which happened at a 3% drift ratio. It can be observed in Fig. 18(a) that the behavior of the longitudinal rebar in the middle column of BCJ-B was symmetrical, with maximum peak resistance occurring at a drift ratio of around ±5%. Specimen BCJ-B also developed a high level of plastic strain after passing peak resistance, which could be attributed to the reduction in the peak resistance triggered by the loss of the concrete section, leading to joint crushing.

Fig. 19 indicates that the measured strain of BCJ-B was symmetrical for negative and positive drift ratios. However, the behavior of column stirrups at the plastic hinge located on the column's longer span was less than yield point for both specimens. This could due to the fact that no plastic strain experienced in both specimens at that particular location of strain for both specimens, or splitting crack occurred causing loss of concrete at longer span of column, leading to shear failure.

The top shear reinforcement rebar within the joint zone, as shown in Fig. 20(a), displayed the tensile strain was yielded under negative cyclic loading. In addition, the magnitude gradually decreased linearly as the negative drift ratio decreased, until the top shear reinforcement behavior increased linearly after achieving a positive drift ratio of 2%. However, for the BCJ-A and BCJ-B specimens, the normalized strain for the second layer from the top of the shear rebar within the joint behave differently in Fig. 20(b). BCJ-B exhibited tensile strain under negative cyclic

(a) Top reinforcement, symbolized by B-L1

(b) Second layer from top reinforcement, symbolized by B-L2

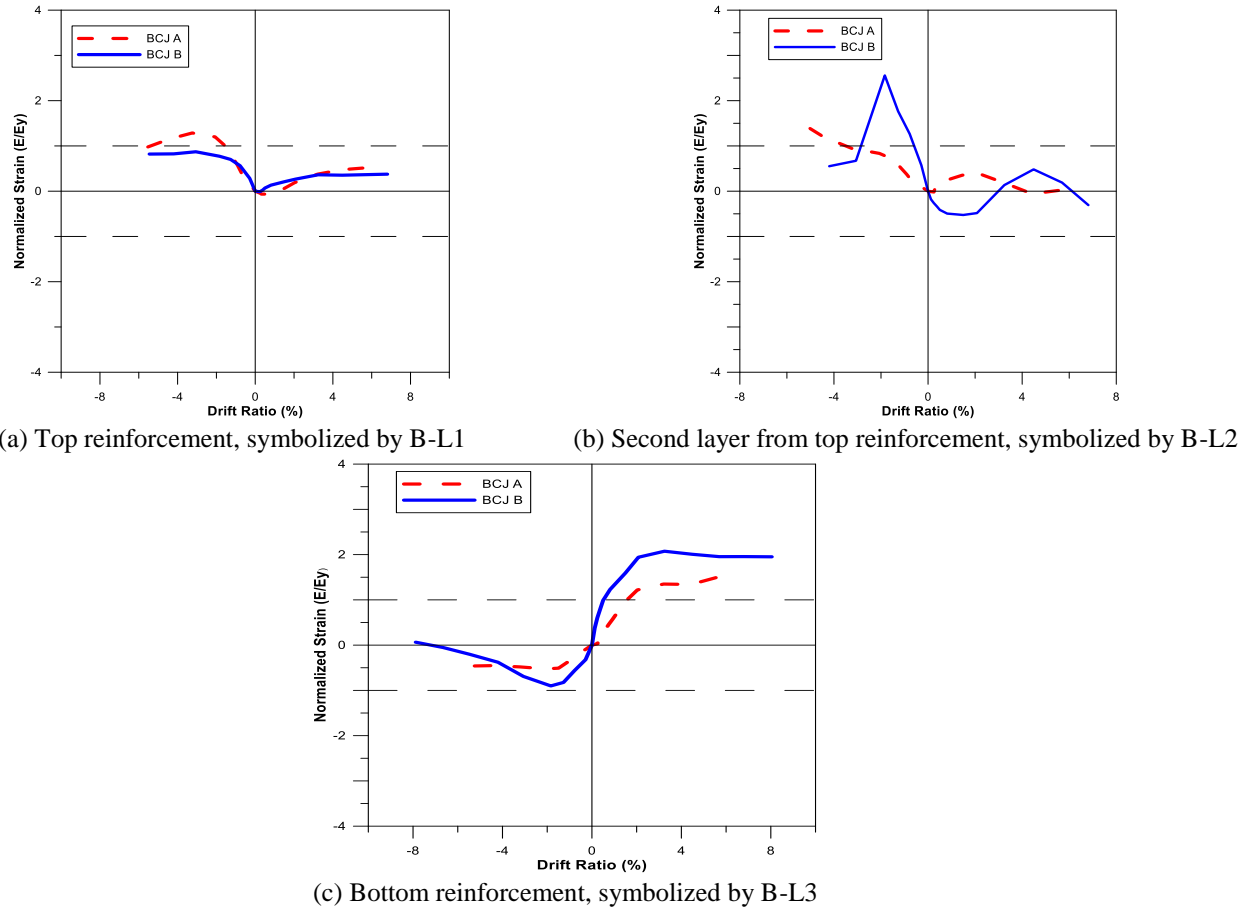(c) Bottom reinforcement, symbolized by B-L3

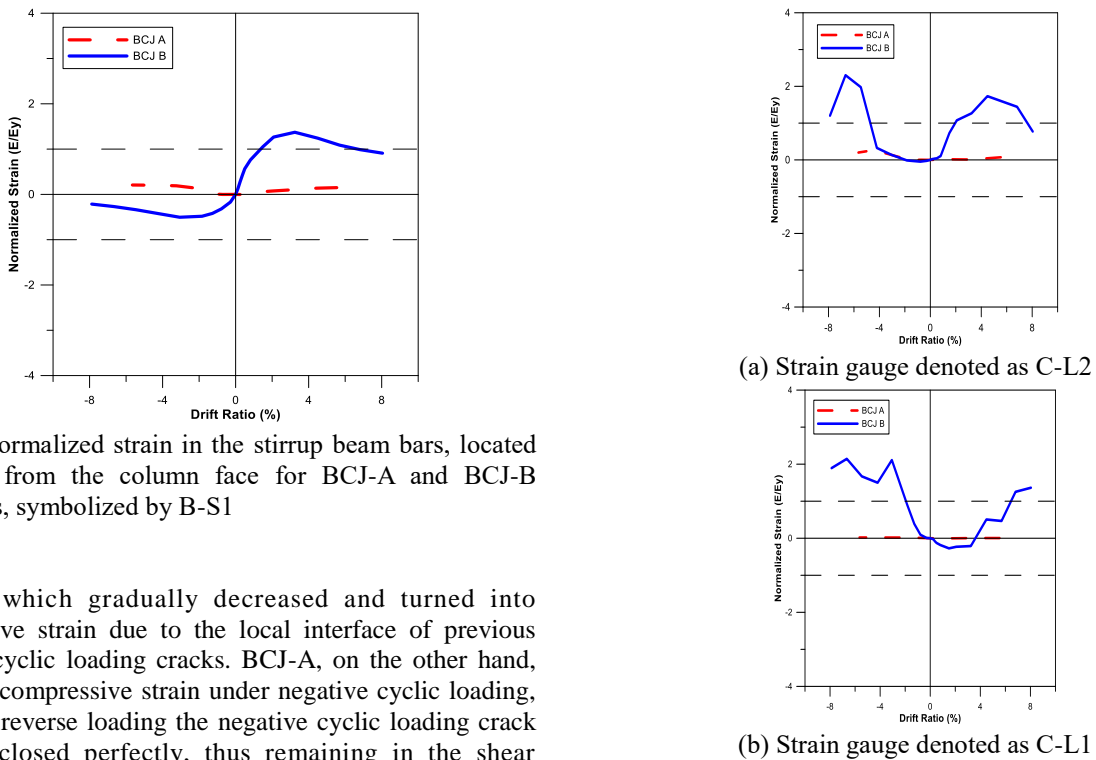Fig. 16 Normalized strain for the beam's longitudinal bars for BCJ-A and BCJ-B specimens, located 25 mm from the column

Fig. 17 Normalized strain in the stirrup beam bars, located 200 mm from the column face for BCJ-A and BCJ-B specimens, symbolized by B-S1

(a) Strain gauge denoted as C-L2

(b) Strain gauge denoted as C-L1

Fig. 18 Normalized strain in the middle of the longitudinal column bars on (a) the shorter side span and (b) the longer side span of the column at the plastic hinge for BCJ specimens

loading, which gradually decreased and turned into compressive strain due to the local interface of previous negative cyclic loading cracks. BCJ-A, on the other hand, exhibited compressive strain under negative cyclic loading, and upon reverse loading the negative cyclic loading crack was not closed perfectly, thus remaining in the shear reinforcement bar. Fig. 20(c) shows that the bottom shear reinforcement within the joint exhibited tensile strain below the yield point in the BCJ-B specimen, which gradually decreased and turned into compressive strain as it reached
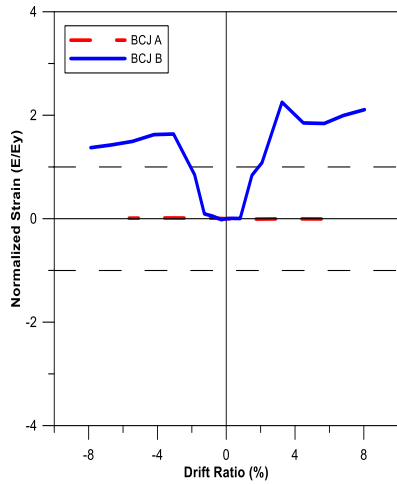
Fig. 19 Normalized strains in the stirrup column for BCJ specimens at the plastic hinge, located on the shorter side of the column, symbolized by C-S2

the yield point. However, BCJ-A was damaged during the application of negative cyclic loading at a specific drift ratio and was unable to exhibit full behavioral result data.

### 3.7 Relation between the joint shear deformation and the drift ratio

The joint shear deformation signifies the nature of the damage induced in the joint based on the increase in cyclic loading, measured in terms of the drift ratio. The shear deformation was determined by selecting four markers of motion tracker devices installed over the joint zone, as displayed in Fig. 21(a). Through geometrical compatibility as illustrated in Fig. 21(b), it was calculated from the measured coordinates position of these markers during the increase in the drift ratio. The shear deformation, denoted as γ, is expressed by Eq. (3), where δ_1 and δ_2 are the change in deformation, and a and b are the shear element width and height, respectively.

$$\gamma = \frac{(\delta_1 + \delta_2)\sqrt{a^2 + b^2}}{2ab} \tag{3}$$

The curve of shear deformation, calculated using Eq. (3) with respect to drift ratio, is shown in Fig. 22. It is clear that the joint shear deformation enhanced with the increment in the drift ratio. The BCJ-A specimen showed a much more substantial shear deformation when the drift ratio was increased compared to the BCJ-B specimen. This is because BCJ-A had a smaller beam–column depth ratio, where failure occurred instantly in the column rather than in the beam, whereas BCJ-B, due to its larger column area, experienced joint failure at a larger drift ratio of 7%. This occurred because there were no stirrups to resist the induced joint force that occurred within the specimen.
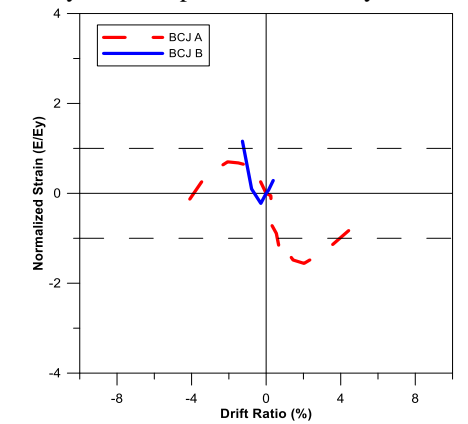
3.8 Joint shear stress

The joint shear stress can be described by principal tensile/compression stress (σ_t, σ_c) or nominal shear stress
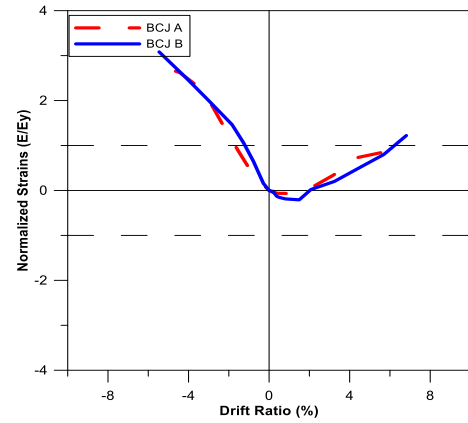
(a) Top reinforcement, symbolized by B-J1
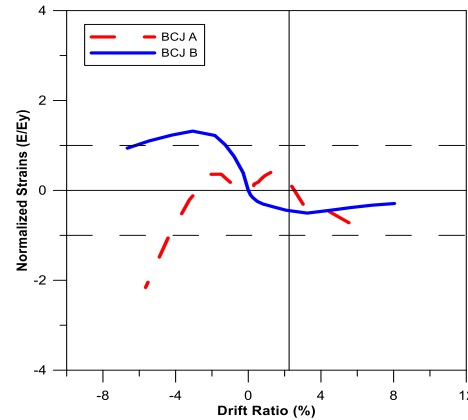
(b) Second layer from top reinforcement, symbolized by B-J2

(c) Bottom reinforcement, symbolized by B-J3

Fig. 20 Normalized strain in beam longitudinal reinforcement within the joint zone

(v_{jh}). This provides more precise representations when taking into account the effect of the actual axial compression stress acting on the column. The horizontal joint shear stress can be estimated through Eq. (4):

$$\upsilon_{jh} = \frac{V_u}{b_c h_c} \leq k\sqrt{f_c'} \tag{4}$$

where V_u denotes the joint shear force which can be defined using Eq. (4), h_c for the depth of the column in the horizontal shear direction considered, b_c is the effective width of the joint, and the factor $k = 0.0083\gamma$ relies on the
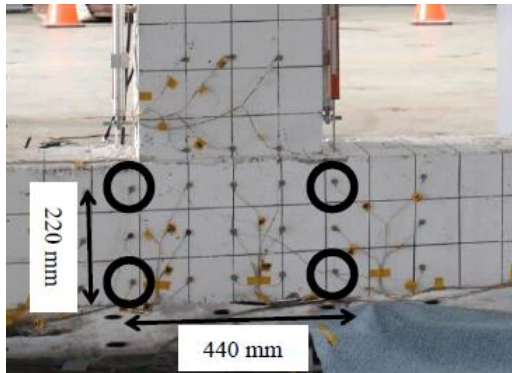
(a) The location of the measurement of joint shear deformation
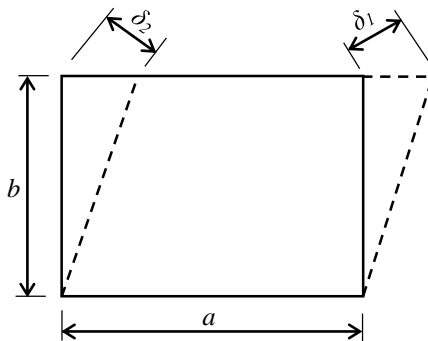
(b) The illustration of geometrical compatibility of the joint shear deformation

Fig. 21 The calculation of the beam–column joint shear deformation

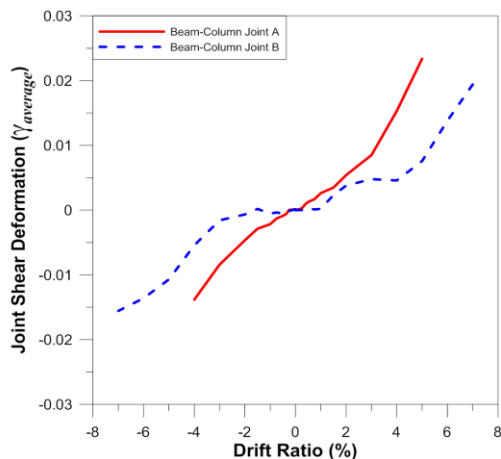Fig. 22 Curves of joint shear deformation versus drift ratio for the beam–column joint

confinement contributed by members enclosing a joint. The limit factor is to protect the joint against diagonal crushing.

Table 3 provides the joint shear stress and the comparison to the limit specified in ACI 318-19 codes (2019). The BCJ-A specimen exhibited 55% higher joint shear stress than the limit due to the mechanism of a weak column with a strong beam, where high stress concentrated on the column caused by concrete spalling is generated by joint shear failure. The BCJ-B specimen also experienced joint shear failure because the value of v_{jh} is 15% greater than the limit specified.

Table 3 Joint shear strength calculation of the BCJ specimens

	$V_{u,ACI}$ (kN)	v_{jh} (kN)	$k\sqrt{f_c'}$
BCJ-A	910	10.10	4.68
BCJ-B	910	5.52	4.68

4. Conclusions

This paper provides an understanding of the seismic behavior of poorly detailed old existing RC frame structures by using the quasi-static testing method. The structural inadequacies are represented by the wider stirrup spacing for the RC columns and lack of joint transverse rebar within the joint for the RC beam–column joints.

The C-A and C-B column specimens failed in the axial flexural mode and shear failure, respectively. The inferior confinement allowed the dilation of the concrete core at a larger drift ratio, which consequently resulted in smaller flexural stresses. The parameters of deformability and energy dissipation also indicated poor performance under seismic load. The ductility factor for the column specimens was found to be lower than the desired value.

In the BCJ specimens, the development of joint shear failure was mainly caused by a lack of joint transverse rebar inside the joint zone, so the shear transfer mechanisms could not develop. The BCJ-A and BCJ-B specimens showed a lower ductility factor than the desired value. The calculation of the joint shear force and joint shear stress also indicates that the BCJ specimens should fail prematurely attributable to joint shear failure. The concept of a strong column with weak beam mechanisms is more effective due to the ability to resist more lateral movement under seismic loading.

References

ACI 318-19 (2019), Building code requirements for structural concrete and commentary, American Concrete Institute; Farmington Hills, MI, U.S.A.

ACI 374.1-05 (2019), Acceptance criteria for moment frames based on structural testing and commentary (reapproved 2019), American Concrete Institute; Farmington Hills, MI, U.S.A.

ACI 374.2R-13 (2013), Guide for testing reinforced concrete structural elements under slowly applied simulated seismic loads, American Concrete Institute; Farmington Hills, MI, U.S.A.

ASTM C39/C39M-20 (2020), "Standard test method for compressive strength of cylindrical concrete specimens", Amer. Soc. Testing Mater, U.S.A. https://doi.org/10.1520/C0039_C0039M-20.

Barbagallo, F., Hamashima, I., Hu, H., Kurata, M. and Nakashima, M. (2017), "Base shear capping buildings with graphite-

lubricated bases for collapse prevention in extreme earthquake", *Earthq. Eng. Struct. D.*, **46**, 1003-1021. https://doi.org/10.1002/eqe.2842.

Benavent-Climent, A. and Zahran, R. (2010), "Seismic evaluation of existing RC frames with wide beams using an energy-based approach", *Earthq. Struct.*, **1**(1), 93-108. http://dx.doi.org/10.12989/eas.2010.1.1.093.

Blume, J.A., Newmark, N.M. and Corning, L.H. (1961), *Design of Multistory Reinforced Concrete Buildings for Earthquake Motions*, Portland Cement Association, Skokie, U.S.A.

Cardone, D. and Flora, A. (2016), "An alternative approach for the seismic rehabilitation RC of existing buildings using seismic isolation", *Earthq. Eng. Struct. D.*, **4**, 91-111. https://doi.org/10.1002/eqe.2618.

Esteghamati, M.Z., Banazadeh, M. and Huang, Q. (2018), "The effect of design drift limit on the seismic performance of RC dual high-rise buildings", *Struct. Des. Tall Spec.*, **27**, 1464. https://doi.org/10.1002/tal.1464.

Faleschini, F., Bragolusi, P., Zanini, M.A., Zampieri, P. and Pellegrino, C. (2017), "Experimental and numerical investigation on the cyclic behavior of RC beam column joints with EAF slag concrete", *Eng. Struct.*, **152**, 332-347. https://doi.org/10.1016/j.engstruct.2017.09.022.

Haach, V.G., De Cresce El Debs, A.L.H. and El Debs, M.K. (2008), "Evaluation of the influence of the column axial load on the behavior of monotonically loaded R/C exterior beam–column joints through numerical simulations", *Eng. Struct.*, **30**(4), 965-975. https://doi.org/10.1016/j.engstruct.2007.06.005.

Hakuto, S., Park, R. and Tanaka, H. (2000), "Seismic load tests on interior and exterior beam-column joints with substandard reinforcing details", *ACI Struct. J.*, **97**(1), 11-25.

Haryanto, Y., Hu, H.T., Han, A.L., Atmajayanti, A.T., Galuh, D.L.C. and Hidayat, B.A. (2019), "Finite element analysis of T-section RC beams strengthened by wire rope in the negative moment region with an addition of steel rebar at the compression block", *J. Teknol.*, **81**(4), 143-154. https://doi.org/10.11113/jt.v81.12974.

Hsiao, F.P., Oktavianus, Y., Ou, Y.C., Luu, C.H. and Hwang, S.J. (2015), "A pushover seismic analysis and retrofitting method applied to low-rise RC school buildings", *Adv. Struct. Eng.*, **18**(3), 311-324. https://doi.org/10.1260/1369-4332.18.3.311.

Hsiao, F.P., Wang, J.C. and Chiou, Y.J. (2008), "Shear strengthening of reinforced concrete framed shear walls using CFRP strips", *Proceedings of the 14th World Conference on Eearthquake Engineering*, Beijing, China, October.

Hsu, T.Y. and Pham, Q.V. (2019), "Post-earthquake assessment of buildings using displacement and acceleration response", *Earthq. Struct.*, **17**(6), 599-609. http://dx.doi.org/10.12989/eas.2019.17.6.599.

Huang, R.Y.C., Kuang, J.S. and Behnam, H. (2018), "Shear strength of exterior wide beam-column joints with different beam reinforcement ratios", *J. Earthq. Eng.*, 1-23. https://doi.org/10.1080/13632469.2018.1545711.

Kaku, T. and Asakusa, H. (1991), "Bond and anchorage of bars in reinforced concrete beam-column joints. Design of beam-column joints for seismic resistance", *ACI SP-123*, American Concrete Institute, Detroit, U.S.A.

Kaku, T. and Asakusa, H. (1991), "Ductility estimation of exterior beam column sub-assemblages in RC frames. Design of beam column joints for seismic resistance", *ACI SP-123*, American Concrete Institute, Detroit, U.S.A.

Kalogeropoulos, G.I., Tsonos, A.D.G., Konstantinidis, D. and Iakovidis, P.E. (2019), "Earthquake-resistant rehabilitation of existing RC structures using high-strength steel fiber-reinforced concrete jackets", *Earthq. Struct.*, **17**(1), 115-129. http://dx.doi.org/10.12989/eas.2019.17.1.115.

Li, B., Siu-Shum Lam, E., Wu, B. and Wang, Y.Y. (2015), "Effect of high axial load on seismic behavior of reinforced concrete beam-column joints with and without strengthening", *ACI Struct. J.*, **112**(6), 713-724. https://doi.org/10.14359/51687938.

Liao, W.C., Perceka, W. and Wang, M. (2017), "Experimental study of cyclic behavior of high-strength reinforced concrete columns with different transverse reinforcement detailing configurations", *Eng. Struct.*, **153**, 290-301. https://doi.org/10.1016/j.engstruct.2017.10.011.

Lu, X., Lu, X., Guan, H. and Ye, L. (2013), "Collapse simulation of reinforced concrete high-rise building induced by extreme earthquakes", *Earthq. Eng. Struct. D.*, **42**, 705-723. https://doi.org/10.1002/eqe.2240.

Lu, X., Urukap, T.H., Li, S. and Lin, F. (2012), "Seismic behavior of interior RC beam-column joints with additional bars under cyclic loading", *Earthq. Struct.*, **3**(1), 37-57. http://dx.doi.org/10.12989/eas.2012.3.1.037.

Mo, Y.L. and Wang, S.J. (2000), "Seismic behavior of RC columns with various tie configurations", J. Struct. Eng., **126**, 112-1130.

Morais, M. and Burgoyne, C. (2001), "Energy dissipation in sections prestressed with FRP tendons", *Proceedings of the Conference of Composites in Constructions*, Porto, Portugal, October.

Pampanin, S., Magenes, G. and Carr, A. (2003), *Modelling of Shear Hinge Mechanism in Poorly Detailed RC Beam-column Joints*, Concrete Structures in Seismic Regions, Athens, Greece.

Pantazopoulou, S. and Bonacci, J. (1992), "Consideration of questions about beam-column joints", *ACI Struct. J.*, **89**(1), 27-36. https://doi.org/10.14359/1281.

Pantelides, C.P., *Lawrence, R.D., Hansen, J. and Nadauld, J. (2002), Assessment of Reinforced Concrete Building Exterior Joints with Substandard Details*, Pacific Earthquake Engineering Research Center, California, U.S.A.

Park, R. and Paulay, T. (1973), "Behaviour of reinforced concrete external beam-column joints under cyclic loading", *Proceedings of the 5th World Conference on Earthquake Engineering*, Rome, Italia, June.

Paulay, T. (1989), "Equilibrium criteria for reinforced concrete beam-column joints", *ACI Struct. J.*, **86**(6), 635-643. https://doi.org/10.14359/2649.

Paulay, T. and Priestley, M.J.N. (1992), *Seismic Design of Reinforced Concrete and Masonry Buildings*, John Wiley & Sons, New York, U.S.A. https://doi.org/10.1002/9780470172841.

Qeshta, I.M., Shafigh, P., Jumaat, M.Z., Abdulla, I.A., Ibrahim, Z. and Alengaram, U.J. (2014), "The use of wire mesh-epoxy composite for enhancing the fexural performance of concrete beams", *Mater. Des.*, **60**, 250-259. https://doi.org/10.1016/j.matdes.2014.03.075.

Rajput, A. and Sharma, K. (2017), "Seismic behavior of under confined square reinforced concrete columns", *Struct.*, **13**, 26-35. https://doi.org/10.1016/j.istruc.2017.10.005.

Shafaei, J., Hisseini, A. and Marefat, M.S. (2014), "Seismic retrofit of external RC beam-column joints by joint enlargement prestressed steel angles", *Eng. Struct.*, **81**, 265-288. https://doi.org/10.1016/j.engstruct.2014.10.006.

Sharma, A., Reddy, G.R., Vaze, K.K. and Eligehausen, R. (2013), "Pushover experiment and analysis of a full scale non-seismically detailed RC structure", *Eng. Struct.*, **46**, 218-233. https://doi.org/10.1016/j.engstruct.2012.08.006.

Sheikh, S.A., Shah, D.V. and Khoury, S.S. (1994), "Confinement of high-strength concrete columns", *ACI Struct. J.*, **91**, 100-111.

Shen, W.C., Hsiao, F.P., Tsai, R.J., Weng, P.W., Li, Y.A. and Hwang, S.J. (2019), "Shaking table test of a reduced-scale reinforced concrete structure subjected to near-fault ground motion", *Proceedings of the Pacific Conference on Earthquake Engineering*, Auckland, New Zealand, April.

Shen, W.C., Hsiao, F.P., Weng, P.W., Li, Y.A., Chou, C.C. and Chung, L.L. (2018), "Seismic tests of a mixed-use residential and commercial building using a novel shaking table", *Proceedings of the 11th US National Conference on Earthquake Engineering*, Los Angelos, USA, June.

Shiravand, M.R., Nashtaee, M.A. and Veismoradi, S. (2017), "Seismic assessment of concrete buildings reinforced with shape memory alloy materials in different stories", *Struct. Des. Tall. Spec.*, **26**, 1384. https://doi.org/10.1002/tal.1384.

Surana, M. (2019), "Evaluation of seismic design provisions for acceleration-sensitive non-structural components", *Earthq. Struct.*, **16**(5), 611-623. http://dx.doi.org/10.12989/eas.2019.16.5.611.

Tsai, K.C., Hsiao, C.P. and Bruneau, M. (2000), "Overview of building damages in the 921 Chi-chi earthquake", *Earthq. Eng. Eng. Seism.*, **2**(1), 93-108.

Tudjono, S., Han, A.L. and Gan, B.S. (2018), "An integrated system for enhancing flexural members' capacity via combinations of the fiber-reinforced plastic use, retrofitting, and surface treatment techniques", *Int. J. Technol.*, **1**, 5-15. https://doi.org/10.14716/ijtech.v9i1.298.

Tudjono, S., Han, A.L. and Hidayat, B.A. (2015), "An experimental study to the influence of fiber-reinforced polymer (FRP) confinement on beams subjected to bending and shear", *Procedia Eng.*, **125**, 1070-1075. https://doi.org/10.1016/j.proeng.2015.11.164.

Wong, H. (2005), "*Shear strength and seismic performance of non-seismically designed reinforced concrete beam-column joints*", Ph.D. Dissertation, Hong Kong University of Science and Technology, Hong Kong. https://doi.org/10.14711/thesis-b914043.

Xiao, Y., Zeng, L., Chen, Y., Du, G., Zhang, J. and Chen, J. (2019), "Seismic fragility analysis of concrete encased frame-reinforced concrete core tube hybrid structure based on quasi-static cyclic test", *Struct. Des. Tall Spec.*, **28**, 1665. https://doi.org/10.1002/tal.1665.

Xue, Q. (2000), "Need of performance-based earthquake engineering in Taiwan: a lesson from the Chi-chi earthquake", Earthq. *Eng. Struct. D.*, **29**, 1609-1627.

Yang, M. and Zhang, C. (2019), "Comparative study on retrofitting strategies for residential buildings after earthquakes", *Earthq. Struct.*, **16**(4), 375-389. http://dx.doi.org/10.12989/eas.2019.16.4.375.

Yen, J.Y. and Chien, H.K. (2004), "Plated RC beam-column joints under cyclic loading", *J. Chin. Inst. Eng.*, **27**(5), 641-650. https://doi.org/10.1080/02533839.2004.9670912.

Yön, B. (2020), "Seismic vulnerability assessment of RC buildings according to the 2007 and 2018 Turkish seismic codes", *Earthq. Struct.*, **18**(6), 709-718. http://dx.doi.org/10.12989/eas.2020.18.6.709.

Zepeda, D. and Hagen, G. (2016), "Lessons learned from the 2016 Taiwan Mei-nong earthquake", *Proceedings of the Structural Engineers Association of California Convention*, Taipei, Taiwan, October.

KT